UCLA
UCLA Previously Published Works

Title
Multi-institutional MicroCT image comparison of image-guided small animal irradiators

Permalink
https://escholarship.org/uc/item/6c45d44r

Journal
Physics in Medicine and Biology, 62(14)

ISSN
0031-9155

Authors
Johnstone, Chris D
Lindsay, Patricia
Graves, Edward E
et al.

Publication Date
2017-07-21

DOI
10.1088/1361-6560/aa76b4

Peer reviewed

Multi-institutional MicroCT image comparison of image-guided small animal irradiators

You may also be interested in:

A quality assurance phantom for the performance evaluation of volumetric micro-CT systems
Louise Y Du, Joseph Umoh, Hristo N Nikolov et al.

Precise image-guided irradiation of small animals: a flexible non-profit platform
Falk Tillner, Prasad Thute, Steffen Löck et al.

Considerations in x-ray CT gel dosimetry
M Hilts, A Jirasek and C Duzenli

Evaluation of a cone beam computed tomography geometry for image guided small animal irradiation
Yidong Yang, Michael Armour, Ken Kang-Hsin Wang et al.

An x-ray image guidance system for small animal stereotactic irradiation
K H Song, R Pidikiti, S Stojadinovic et al.

A multipurpose quality assurance phantom for the small animal radiation research platform (SARRP)
Wilfred Ngwa, Panagiotis Tsiamas, Piotr Zygmanski et al.

Validation of fast Monte Carlo dose calculation in small animal radiotherapy with EBT3 radiochromic films
C Noblet, S Chiavassa, F Smekens et al.

Multi-institutional MicroCT image comparison of image-guided small animal irradiators

Chris D Johnstone[1], **Patricia Lindsay**[2,3], **Edward E Graves**[4],
Eugene Wong[5], **Jessica R Perez**[6], **Yannick Poirier**[7],
Youssef Ben-Bouchta[8], **Thilakshan Kanesalingam**[9],
Haijian Chen[10], **Ashley E Rubinstein**[11] ⓘ, **Ke Sheng**[12]
and Magdalena Bazalova-Carter[1,13]

[1] Department of Physics and Astronomy, University of Victoria, Victoria, BC, Canada
[2] Radiation Medicine Program, Princess Margaret Cancer Centre, University Health Network, Toronto, ON, Canada
[3] Department of Radiation Oncology, University of Toronto, Toronto, ON, Canada
[4] Department of Radiation Oncology, Stanford University, Stanford, CA, United States of America
[5] Department of Physics and Astronomy, University of Western Ontario, London, ON, Canada
[6] Medical Physics Unit, McGill University, Montreal, QC, Canada
[7] Department of Radiation Oncology, University of Maryland School of Medicine, Baltimore, MD, United States of America
[8] Department of Medical Physics, British Columbia Cancer Agency, Vancouver, BC, Canada
[9] Xstrahl Inc., Atlanta, GA, United States of America
[10] Department of Radiation Oncology, Dana-Farber Cancer Institute and Harvard Medical School, Boston, MA, United States of America
[11] Department of Radiation Physics, University of Texas, MD Anderson Cancer Center, Houston, TX, United States of America
[12] Department of Radiation Oncology, University of California, Los Angeles, CA, United States of America

E-mail: bazalova@uvic.ca

Abstract

To recommend imaging protocols and establish tolerance levels for microCT image quality assurance (QA) performed on conformal image-guided small animal irradiators. A fully automated QA software SAPA (small animal

[13] DABR Assistant Professor and Canada Research Chair (Tier 2) Department of Physics and Astronomy University of Victoria Victoria, British Columbia V8P 5C1, Canada.

phantom analyzer) for image analysis of the commercial Shelley micro-CT MCTP 610 phantom was developed, in which quantitative analyses of CT number linearity, signal-to-noise ratio (SNR), uniformity and noise, geometric accuracy, spatial resolution by means of modulation transfer function (MTF), and CT contrast were performed. Phantom microCT scans from eleven institutions acquired with four image-guided small animal irradiator units (including the commercial PXi X-RAD SmART and Xstrahl SARRP systems) with varying parameters used for routine small animal imaging were analyzed. Multi-institutional data sets were compared using SAPA, based on which tolerance levels for each QA test were established and imaging protocols for QA were recommended. By analyzing microCT data from 11 institutions, we established image QA tolerance levels for all image quality tests. CT number linearity set to $R^2 > 0.990$ was acceptable in microCT data acquired at all but three institutions. Acceptable SNR > 36 and noise levels <55 HU were obtained at five of the eleven institutions, where failing scans were acquired with current-exposure time of less than 120 mAs. Acceptable spatial resolution (>1.5 lp mm^{-1} for MTF $= 0.2$) was obtained at all but four institutions due to their large image voxel size used (>0.275 mm). Ten of the eleven institutions passed the set QA tolerance for geometric accuracy ($<1.5\%$) and nine of the eleven institutions passed the QA tolerance for contrast (>2000 HU for 30 mgI ml^{-1}). We recommend performing imaging QA with 70 kVp, 1.5 mA, 120 s imaging time, 0.20 mm voxel size, and a frame rate of 5 fps for the PXi X-RAD SmART. For the Xstrahl SARRP, we recommend using 60 kVp, 1.0 mA, 240 s imaging time, 0.20 mm voxel size, and 6 fps. These imaging protocols should result in high quality images that pass the set tolerance levels on all systems. Average SAPA computation time for complete QA analysis for a 0.20 mm voxel, 400 slice Shelley phantom microCT data set was less than 20 s. We present image quality assurance recommendations for image-guided small animal radiotherapy systems that can aid researchers in maintaining high image quality, allowing for spatially precise conformal dose delivery to small animals.

Keywords: small animal irradiator, microCT, quality assurance, quantitative imaging, software

(Some figures may appear in colour only in the online journal)

1. Introduction

The use of conformal small animal irradiators advances the ability to treat human cancers with radiation through preclinical trials. Performing accurate irradiation on small animals gives a better understanding of radiation responses of normal and tumorous tissues, where preclinical studies on the effects of new treatment and fractionation schemes for major anatomical sites (e.g. brain, lung, pancreas, liver, colon, prostate) can be efficiently carried out in a controlled setting (Redmond *et al* 2011, Baumann *et al* 2012, Barton *et al* 2013, Burrell *et al* 2013, Lee *et al* 2013, Bazalova and Graves 2014, Herter-sprie *et al* 2014). Coupling radiation with drugs, surgery, and/or nanoparticle delivery can help produce a valuable understanding of cross-modality treatments that otherwise would not be possible without small animal models (Lo *et al* 2012, Chattopadhyay *et al* 2013, Zeng *et al* 2013, Mahmood *et al* 2014, Kunjachan

et al 2015). Studies using the relatively short lifetimes of small animals are advantageous, as similar patient follow-up studies may take decades to acquire and can lack the regulation of a controlled setting.

Preclinical treatments require submillimeter precision to minimize dose to the small critical structures of the animal, where a close match between delivered and prescribed dose must be achieved. These submillimeter requirements for highly accurate and reproducible radiation guidance are facilitated by means of microCT imaging. Thus, high-resolution imaging is essential for image-guided small animal radiotherapy systems and there is a need for establishing standards in image quality. Unlike the American Association of Physicists in Medicine Task Group (AAPM TG) 179 for the QA of CT-based image-guided accelerators (Bissonnette *et al* 2012), an equivalent does not yet exist for microCT-based image-guided small animal irradiators.

There are currently two companies manufacturing image-guided small animal irradiators: Precision x-ray Incorporated (PXi, North Brandford, CT) and Xstrahl Inc. (Xstrahl, Suwanee, GA). In this paper, microCT images of the commercial PXi X-RAD SmART and Xstrahl Small Animal Radiation Research Platform (SARRP) irradiators, as well as two in-house built systems, GE eXplore CT/RT 140 and GE eXplore CT120 (GE Healthcare, Milwaukee, WI), were investigated. A detailed summary of the specifications of each system are available (Verhaegen *et al* 2011), and briefly described in section 2.3.

Image quality characterization of small animal irradiators has been carried out in a past study presenting data from a single institution and irradiator (Clarkson *et al* 2011). Clarkson *et al* covered a limited number of variable microCT imaging parameters and obtained image quality and reproducibility results from their image-guided small animal irradiator. This manuscript encompasses and compares data from eleven institutions and four different image-guided small animal irradiators, acquired with a range of imaging protocols.

This work presents important steps towards comprehensive imaging QA for image-guided small animal radiotherapy. Here we respond to the lack of standardized imaging QA protocols for image-guided small animal irradiators and we illustrate a large range of image quality differences among institutions. To our knowledge, this is the first and most extensive multi-institutional study of its kind that presents microCT image quality of image-guided small animal irradiators and recommends imaging QA protocols and achievable tolerance levels.

2. Materials and methods

A fully automated in-house QA small animal phantom analyzer (SAPA) software for quantitative analysis of the Micro-CT MCTP 610 phantom (Shelley Medical Imaging Technologies, London, ON, here referred to as the Shelley phantom) (Du *et al* 2007), was created in Matlab (The Mathworks, Nattick, MA). This phantom was specifically designed to be used as a device to assess image quality of microCT scanners. The Shelley phantom consists of six cylindrical polycarbonate plates containing CT number linearity, uniformity and noise, geometric accuracy, spatial resolution with slanted edge, spatial resolution with contrast coils, and CT number evaluation plates, as illustrated in figure 1. The total phantom length and diameter are 9 and 7 cm, respectively.

2.1. SAPA

The SAPA software carries out quantitative analysis of CT linearity, signal-to-noise ratio (SNR), uniformity and noise, geometric accuracy, spatial resolution using the modulation transfer function (MTF), and CT number evaluation, completely independent of the user. The SAPA graphical user interface (GUI) is presented in figure 2. The quantification of all image
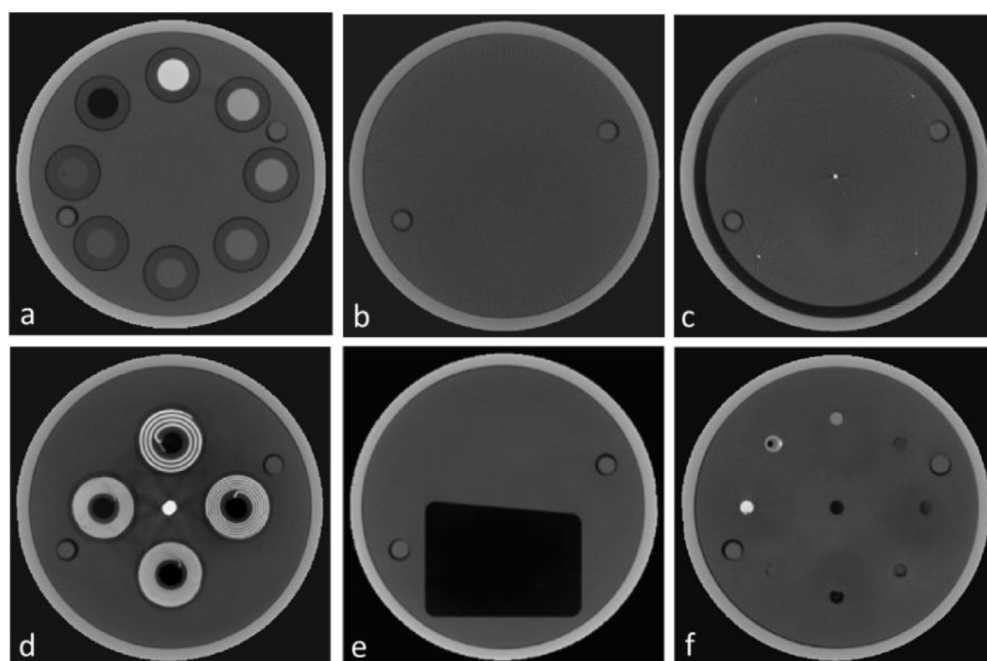
Figure 1. MicroCT images of the six quality assurance plates of the Shelley phantom after alignment in SAPA, illustrating the (a) CT number linearity plate, (b) uniformity and noise plate, (c) geometric accuracy plate, (d) spatial resolution coil plate, (e) spatial resolution slanted edge plate, and (f) CT number evaluation plate.

quality metrics were carried out based on methods introduced in a past study (Du *et al* 2007), and are briefly described in section 2.2.

After the user selects the directory containing the phantom microCT images, the physical locations of the six QA plates within the Shelley phantom are automatically detected. SAPA then aligns the phantom in the same fashion for every scan regardless of the phantom's original orientation on the couch, to be displayed to the user in the slab order and orientation as shown in figure 1. For this alignment, the images are rotated (the highest 30 mg ml^{-1} iodine concentration of the CT number linearity plate is positioned at 12 o'clock), cropped so the edge of the phantom is within 2 mm from the edge of the frame, and a mask is applied to the area outside the phantom to remove any outside artifacts. When needed, the images are then mirrored and the image order is reversed to achieve the standard phantom orientation for image analysis. In other words, the phantom may be scanned in any orientation and visual image quality assessment of any QA plate over multiple data sets can be easily performed in SAPA. Image quality parameters calculated after phantom alignment were within measurement error when compared to calculations without phantom alignment. All CT numbers are converted to Hounsfield Units (HU) through linear interpolation using the air and water vials in the CT linearity plate, where air and water are set to -1000 and 0 HUs, respectively. SAPA then carries out each QA test by acquiring the necessary volumes of interest (VOIs) for each QA plate, as described in section 2.2. Quantitative QA results are then displayed in the GUI as shown in figure 2. Each QA plate can be scrolled through in the viewer and the VOIs used for computation of each specific test are displayed. The user can also change the display window and level settings.

Additional functionalities of SAPA include the options to export the raw numerical QA data into a Microsoft Excel spreadsheet, obtain header information of scans, and save images
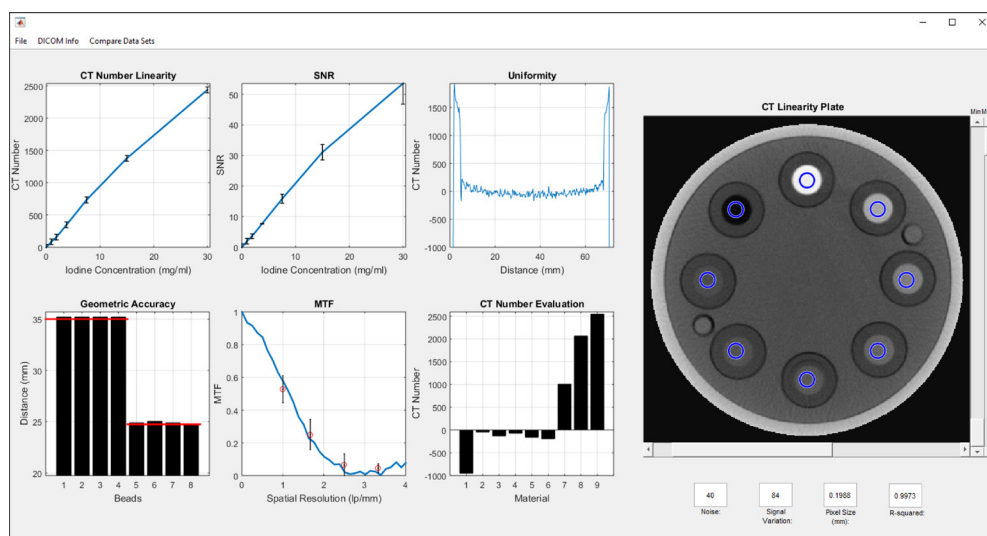
Figure 2. Screenshot of SAPA, our fully automated in-house QA software's graphical user interface for QA analysis of the MCTP 610 Shelley phantom. Upon opening MicroCT scans in SAPA, image analysis of CT number linearity, SNR, uniformity, noise, geometric accuracy, MTF, and CT number evaluation are automatically calculated, independent of user, with an average computation time of less than 20 s. ROIs and MicroCT slices used for calculation are displayed to the user. Multiple analyses can be exported and compared to see if image quality degrades over time.

of slices as tagged image file format (TIFF) files. SAPA can also automatically compare saved quantitative QA data from multiple datasets. This comparison can be used to display changes in a system's imaging functionality from its original performance and/or from the recommended tolerance levels presented in this study.

Users of the Shelley phantom also have the option of conducting image analysis for QA manually, or with image analysis software provided by the manufacturer of the Shelley Phantom (Model vmCT-SOFT). However, the manufacture's software is proprietary and does not have the ability to directly compare QA results in the fashion that SAPA stores data over time.

2.2. Imaging parameters

2.2.1. CT number linearity and SNR. CT number linearity was evaluated using the CT number linearity plate containing six vials of iodine solutions with concentrations of 0.9375, 1.875, 3.75, 7.5, 15, and 30 mgI ml^{-1}. The air and water vials of the CT number linearity plate were used for HU calibration, as described above. Signal intensities in HUs were obtained from a cylindrical VOI that was 3 mm in diameter and 3 mm in depth (throughout the paper represented as 3Ø × 3 mm^3 VOI) within each vial, and plotted as a function of iodine concentration. Next, the coefficient of determination (R^2) for a linear data fit was calculated, where a value of $R^2 = 1$ indicated that the data was perfectly linear. SNR was obtained as the ratio between mean signal intensity and signal variation expressed by means of HU standard deviation within the same VOIs.

2.2.2. Uniformity and noise. Image uniformity was evaluated by plotting a line profile through the center of the uniformity plate. Signal uniformity was also obtained by calculating the signal intensity difference between four 5Ø × 3 mm^3 peripheral VOIs and a central

$5\varnothing \times 3\,mm^3$ VOI. In addition, image noise was obtained as the average of the standard deviation within the five VOIs.

2.2.3. Geometric accuracy. The geometric accuracy plate was designed with five 280 μm diameter tungsten-carbide beads to determine the in-plane voxel size of the reconstructed microCT volume. The respective distances of the beads were measured for the evaluation of geometric accuracy. Four of the corner beads are 35 mm apart and the central bead is located 24.75 mm from the four corner beads. The in-plane voxel size was determined by dividing the known physical distance between neighboring beads by the measured distance between the centroid of the respective neighboring beads in voxels.

2.2.4. Spatial resolution. Spatial resolution was obtained in two ways, using the resolution coil plate and the slanted edge plate. The resolution coil plate has four coils of alternating aluminum and plastic sheets with 500, 300, 200, and 150 μm thicknesses, corresponding to spatial resolution of 1, 1.67, 2.5, and 3.3 lp mm^{-1}, respectively. MTF can be determined by using the standard deviation of pixel values from ROIs within a cyclic bar pattern (e.g. each coil), as calculated by the following equation (Droege and Morin 1982),

$$\mathrm{MTF}(f) = \frac{\pi\sqrt{2}}{4} \cdot \frac{M(f)}{M_o}, \tag{1}$$

where $M(f)$ is the average standard deviation of four $2\varnothing \times 3\,mm^3$ VOIs taken within each coil and corrected for noise, and M_o is half of the absolute difference between the aluminum and plastic HUs. MTF was also obtained with the slanted edge method (Judy 1976), where the slanted edge is created by an air-polycarbonate plastic boundary and is tilted by 5° in order to create sub-pixel edge positions. A profile through the slanted edge defines the edge-spread function (ESF), and when differentiated, the line spread function (LSF) is obtained. Finally, the MTF is determined by calculating the Fourier transform of the LSF. In SAPA, the MTF from the coil resolution plate is plotted with the MTF obtained from the slanted edge test (figure 2). Unlike in the resolution coil test, the slanted edge MTF analysis results in continuous frequency values ranging from 0.0 to 3.3 lp mm^{-1}.

2.2.5. CT number evaluation and image contrast. Finally, the CT number evaluation plate was used to analyze the output of the system in HUs by means of nine tissue-equivalent materials embedded in the Shelley phantom. The mean HU of nine $1.5\varnothing \times 3\,mm^3$ VOIs of each material were plotted. Analysis of the CT number evaluation plate proved to be difficult, as the Shelley phantom's nine tissue-equivalent materials were sparse and non-uniform within and across slices. The vials often included a material non-uniformity, both within the center, edges, and entire length of each vial, making accurate measurements challenging and problematic to reproduce. While the CT number evaluation plate data was plotted in SAPA, for QA purposes, iodine vials from the CT number linearity plate were used to assess changes in CT numbers and the 30 mgI ml^{-1} vial was used as the metric for image contrast.

2.3. Image-guided small animal irradiators

2.3.1. PXi X-RAD SmART. MicroCT imaging in the PXi X-RAD SmART system, previously sold as the 225cX system, is performed with a 360°-rotation of the C-arm gantry using cone beam CT (CBCT) geometry (figure 3(a)). Focal spot x-ray beams of 3.0 and 0.4 mm are used for therapy and imaging, respectively, and are calibrated to a 30.7 cm source-to-isocenter
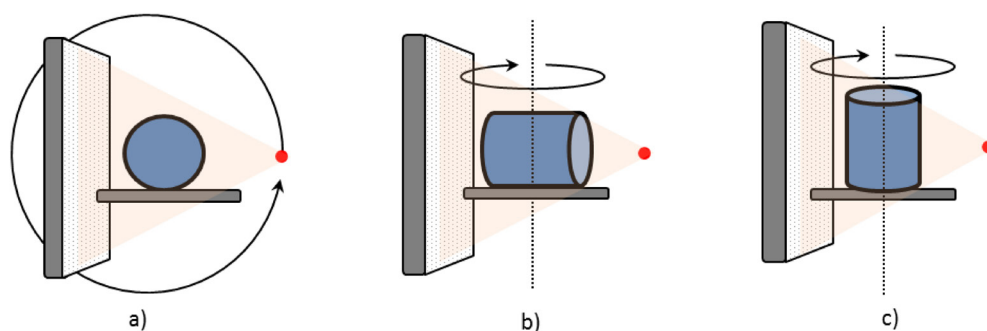
Figure 3. Illustrated is the (a) PXi X-RAD SmART and conventional CBCT imaging geometry, with a stationary table as both source and detector rotate 360° around the short-axis of phantom. This is in comparison to the Xstrahl SARRP with stationary source and detector, as the table rotates 360° with (b) phantom lying down in 'pancake' geometry (photons transverse long and short-axes of phantom) and (c) phantom standing up in standard geometry (photons transverse only short-axis of phantom), more similar to conventional CBCT geometry.

distance (SID) and 64.5 cm source-to-detector distance (SDD) (Clarkson *et al* 2011, Van Hoof *et al* 2013). The PXi X-RAD SmART system utilizes an amorphous silicon flat-panel detector with a pixel size of 200 μm (Perkin-Elmer, Wiesbaden, Germany) that captures x-rays generated with tube voltages generally between 40 and 100 kVp. The PXi X-RAD SmART system performs radiation therapy a tube voltage of 220 kVp and tube current of 13 mA, using 1–25 mm diameter circular and 5×5 to 40×40 mm^2 square field collimators as well as a motorized rotating collimator with a 4 Gy min^{-1} maximum output (Clarkson *et al* 2011).

2.3.2. Xstrahl SARRP. MicroCT imaging on the Xstrahl SARRP is acquired in the so-called 'pancake' geometry (figure 3(b)) with a stationary x-ray tube and detector with a 360° rotating couch. To obtain a more conventional CBCT geometry, the phantom may be placed standing on the couch (figure 3(c)). The SID and SDD are 35 cm and 50 cm, respectively. The x-ray tube operates with a dual focal spot of 3.0 and 0.4 mm for therapy and imaging, respectively (Wong *et al* 2008, Tryggestad *et al* 2009). The Xstrahl SARRP system utilizes the aforementioned Perkin-Elmer detector as well and acquires microCT images with tube voltages between 40 and 80 kVp. Alternatively, a Varian 252DX panel with a pixel size of 127 μm can be used for imaging. Radiation therapy is performed a tube voltage of 220 kVp and tube current of 13 mA, using 0.5–10 mm diameter circular and 3×3 to 10×10 mm^2 square collimators with a 4 Gy min^{-1} maximum output. A motorized variable collimator capable of rectangular field sizes from 1×1 mm^2 to 40×80 mm^2 is also available.

2.3.3. GE eXplore CT 120 and CT/RT 140. The GE eXplore CT120 (GE Healthcare, London, Ontario, Canada) was adapted to radiotherapy delivery by adding a two-stage iris collimation system (Rodriguez *et al* 2009). This system utilizes a pulsed x-ray beam running a ~10% duty cycle with a 0.3 mm focal spot for imaging, in contrast to using a continuous imaging beam on the PXi and Xstrahl units (Zhou *et al* 2010). The amorphous silicon flat panel detector has a pixel size of 49 μm and the SID and SSD are 35.4 cm and a 45 cm, respectively. MicroCT imaging on the GE eXplore CT120 scanner is performed with tube voltages between 70 and

120 kVp and radiotherapy with the maximum tube voltage of 120 kVp and tube current of 60 mA, using 1–10 cm diameter circular collimation with ~2 Gy min^{-1} maximum output. The GE eXplore CT/RT140 microCT imaging is performed in similar fashion to the imager of the GE eXplore CT120 scanner (Jensen *et al* 2013). Radiotherapy is performed at 140 kVp with a 1.0 mm focal spot with a set of computerized independent jaws and the same SID as the eXplore CT120.

2.4. Multi-institutional study

To identify suitable imaging parameters and establish tolerance levels for microCT imaging QA tests of image-guided small animal irradiators, we analyzed microCT images of the same Shelley phantom scanned at eleven institutions. Each institution submitted multiple microCT data sets with varying imaging parameters, where the data sets acquired with imaging parameters routinely used for small animal radiotherapy were used in this study. Chosen imaging protocols for all institutions ranged from using manufacturer recommendations developed during irradiator commissioning, to institution-specific imaging research and techniques of past small animal studies, or a mixture of these. As stated above, four different irradiator units were involved in the study, the PXi X-RAD SmART, Xstrahl SARRP, GE Explore CT120, and GE Explore CT/RT 140. In no particular order, the institutions involved in this study were: Dana-Farber Cancer Institute, University of Maryland, University of Western Ontario, University of Victoria, Princess Margaret Cancer Centre, University of California, Los Angeles, McGill University, MD Anderson Cancer Center, Stanford University, BC Cancer Agency-Vancouver Centre, and Xstrahl Inc. Imaging parameters used to acquire the presented data at the eleven institutions are summarized in table 1.

We compared image quality parameters of the entire multi-institutional data set and established tolerance levels for each QA test based on the comparative performance of the systems, described in section 3.2. Note that the Shelley phantom was scanned in the 'pancake' geometry (figure 3(b), phantom lying on the couch), as opposed to the standard imaging geometry (figure 3(c), phantom standing on the couch) on all Xstrahl SARRP irradiators of the multi-institutional study. In order to investigate the effects of imaging geometry, we also compared image quality for the standard imaging geometry with the 'pancake' imaging geometry employed with the Xstrahl SARRP at two institutions. This comparison was done by laying the Shelley phantom on the couch for 'pancake' geometry and repeated using the same imaging parameters with the Shelley phantom standing on the couch achieving the standard imaging geometry.

2.5. SAPA validation

SAPA imaging parameter evaluation results were validated against hand calculations assisted with Fiji (Schindelin *et al* 2012), a distribution of the open-source software ImageJ (Abràmofff *et al* 2004), and independent Matlab code. Regions of interests (ROIs) of approximately the same size used in SAPA were acquired using Fiji, and the QA results were obtained in the same fashion as described in section 2.2. for CT number linearity, SNR, uniformity and noise, geometric accuracy, MTF (resolution coil plate), and CT evaluation number. MTF (slanted edge plate) was acquired with independent Matlab code specifically designed to acquire the MTF of a slanted edge, where the user manually defines an ROI composed of approximately 50% air and 50% plastic within the slanged edge plate.

Table 1. Imaging parameters and irradiators used in the multi-institutional study.

Institution	Voltage (kVp)	Added +filtration (mm Al)	Current (mA)	Total imaging Time (s)	Current-exposure time (mAs)	Voxel size (mm)	Irradiator
Institution 1	70	2.0	3.0	60	180	0.200	SmART
Institution 2	60	1.0	0.8	240	192	0.200	SARRP
Institution 3	60	4.5 + 0.38 Cu[a]	63	240[b]	1008[b]	0.205	eXplore 140
Institution 4	60	2.0	1.0	120	120	0.200	SmART
Institution 5	70	4.5	40	240[b]	480[b]	0.192	eXplore 120
Institution 6	65	1.0	0.9	60	54	0.350	SARRP
Institution 7	60	2.0	4.0	20	80	0.150	SmART
Institution 8	60	1.0	0.8	240	192	0.325	SARRP
Institution 9	60	1.0	0.7	57	40	0.275	SARRP
Institution 10	60	1.0	0.8	60	48	0.325	SARRP
Institution 11	80	2.0	2.0	120	240	0.200	SmART

[a] Addition of 0.38 mm Cu filtration reduces mouse imaging dose by approximately 10%.
[b] Pulsed beam with ~10% duty cycle. Listed voxel sizes are identical in all three directions for all institutions, except institution 3 (0.205×0.205 mm^2 in the transverse plane, 0.478 mm along the longitudinal axis).
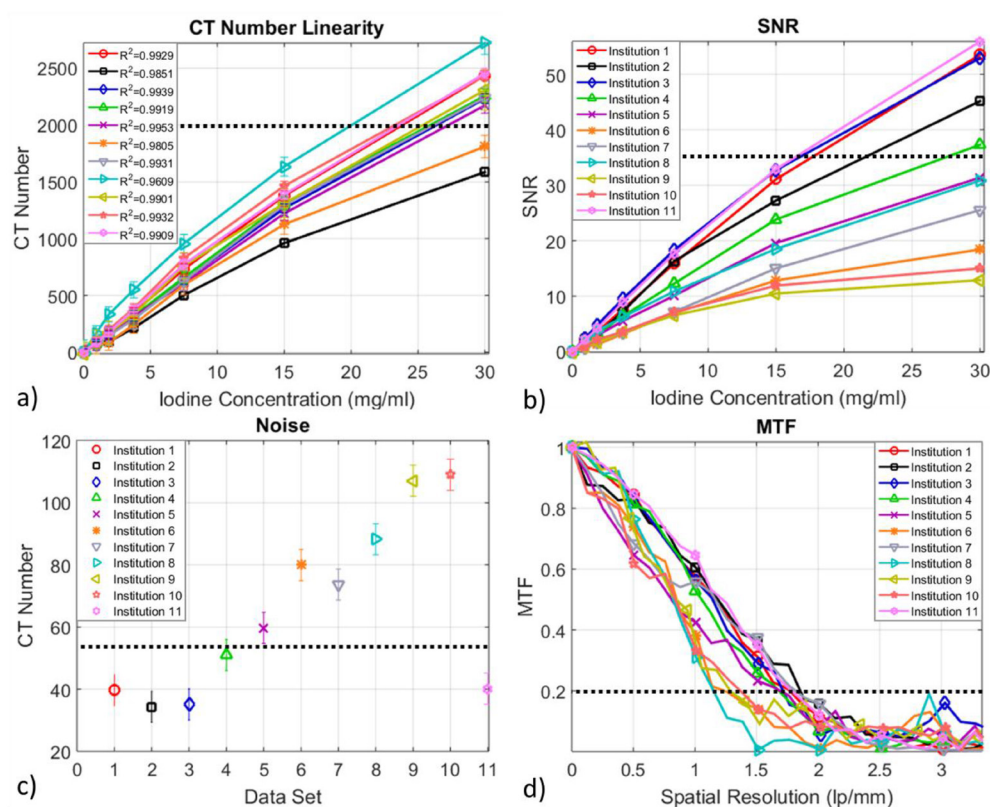
3. Results

3.1. Multi-institutional study

MicroCT image quality parameters from the multi-institutional study performed with the Shelley phantom and analyzed with SAPA are plotted in figure 4. CT number linearity, expressed in terms of R^2 of the linear fit, ranged from 0.9609 to 9953. The values of SNR for the 30 mgI ml^{-1} vial ranged among the data sets from 12 to 56, and noise levels also ranged from 35 to 110 HU. The spatial frequency for MTF = 0.2 ranged from 1.15 lp mm^{-1} to 1.82 lp mm^{-1}. The geometric accuracy, expressed as the difference between the nominal and measured voxel size, ranged from 0.1% to 2.2%. Image contrast for the 30 mgI ml^{-1} varied from 1585 to 2721 HU.

3.2. Tolerance level recommendations

Based on the multi-institutional study presented in figure 4, tolerance levels for microCT QA tests were established for CT number linearity, SNR, noise, MTF (slanted edge), geometric accuracy, and image contrast and are summarized in table 2. Tolerance levels were established based on the comparative performance of the institutions and the justification of their choice is described in the following paragraph.

CT linearity (figure 4(a)) had an R^2 range between 0.9609 and 0.9953, where the poorest linearity ($R^2 < 0.990$) occurred for data sets with the apparent outliers with lowest (HU < 2000, Institutions 2 and 6) and highest (HU > 2500, Institution 8) values for the 30 mgI ml^{-1}. As a result, CT linearity tolerance level of $R^2 > 0.990$ was established. SNR (figure 4(b)) and noise (figure 4(c)) tolerance levels were established in concert, as the two imaging parameters are related. SNR values of >36 were achieved at five institutions (Institutions 1, 2, 3, 4, 11), which corresponded to noise values of <55 HU at the same five institutions. It should be noted that based on a previous study (Bazalova and Graves 2011), CT noise lower than 55 HU is required to keep MC dose calculation accuracy of the 220 kV SARRP beam within 5%. For

Figure 4. Multi-institutional study results for (a) CT number linearity, (b) SNR, (c) noise, and (d) slanted edge MTF acquired at eleven institutions. Tolerance levels for each QA test were established in section 3.2 and are represented by the dashed horizontal lines.

Table 2. Recommended tolerance levels for image quality assurance of image-guided small animal irradiators.

	CT# linearity R^2	Noise	SNR	MTF	Geometric accuracy	Contrast
			30 mgI ml^{-1}	0.2	Bead distance, voxels	30 mgI ml^{-1}
Tolerance	>0.990	<55 HU	>36	>1.5 lp mm^{-1}	±0.20 mm, <1.5%	>2000 HU

our 2000 HU contrast tolerance level within the 30 mgI ml^{-1} vial, this correlates to an SNR of 36 (2000 HU/55 HU). Therefore we chose to set SNR and noise tolerance levels to be >36 and <55 HU, respectively. The MTF plot (figure 4(d)) shows two noticeable groups of curves separated by 1.5 lp mm^{-1} at 20% MTF. The four lower-resolution curves were obtained with voxel sizes of 0.275 mm or greater and degradation in resolution could be observed with voxel sizes of 0.275 mm. As a result, spatial resolution tolerance level of >1.5 lp mm^{-1} at the 20% mark in MTF was established. Geometric accuracy was within a 1.5% difference (less than 0.20 mm) for all data sets except one (2.2% difference, Institution 7). Along with 0.20 mm as our recommendation for voxel size, a tolerance level of 1.5% was established. Finally, image contrast expressed as the CT number of the 30 mgI ml^{-1} vial ranged from 1585 to 2721 HUs.

Table 3. Multi-institutional study summary: Institution and irradiator pass rate for set imaging QA tolerance levels.

Pass Rate	Linearity $R^2 > 0.990$	Noise <55 HU	SNR > 36 30 mgI ml^{-1}	>1.5 lp mm^{-1} @ MTF $= 0.2$	Geometric Accuracy $< 1.5\%$	Contrast > 2000 HU @30 mgI ml^{-1}
Institution	8/11	5/11	5/11	7/11	10/11	9/11
SmART	4/4	3/4	3/4	4/4	3/4	4/4
SARRP	2/5	1/5	1/5	1/5	5/5	3/5
eXplore	2/2	1/2	1/2	2/2	2/2	2/2

Table 4. Recommended QA imaging parameters using the Shelley phantom.

	Voltage (kVp)	Total imaging time (s)	Current (mA)	Voxel size (mm)	Frame rate (fps)
SmART	70	120	1.5	0.20	5
SARRP[a]	60	240	1.0	0.20	6

[a]We recommend scanning the Shelley phantom in the standard geometry in the SARRP system.

Two outliers with image contrast of <2000 HU could be identified in figure 4(a), and therefore the image contrast tolerance level was set as >2000 HU.

Table 3 summarizes the number of institutions passing the set QA tolerance levels for each test, as well as for the different irradiators. Note that microCT data sets acquired at four (Institution 1, 3, 4, 11) of the eleven institutions passed all set tolerance levels.

3.3. Imaging QA protocol recommendations

Based on an extensive image quality study of the two commercial irradiators, the PXi X-RAD SmART and the Xstrahl SARRP system, we recommend performing imaging QA with the Shelley phantom using the scanning protocols summarized in table 4. These recommended parameters were deemed to be the optimal combination to ensure all imaging tolerance levels are met in a single scan. When the recommended parameters of table 4 were employed during additional data acquisitions at Institutions 1, 8, 10, and 11, all QA tests passed the set tolerance levels.

3.4. SARRP 'pancake' and standard imaging geometry comparison

Results comparing the 'pancake' imaging geometry (figure 3(b)) with the Xstrahl SARRP standard imaging geometry (figure 3(c)) using data acquired at two institutions are presented in figure 5.

Standard imaging geometry at both institutions produced passing linearity ($R^2 > 0.990$) where the 'pancake' imaging geometries failed. Image noise was 20% and 35% lower in the standard geometry for institutions A and B, respectively. Likewise, SNR was 40% and 25% higher for the standard geometry. On the other hand, spatial resolution at MTF $= 0.2$ was 30% and 8% higher in the 'pancake' geometry for Institutions A and B, respectively. Geometric accuracy was within error bars for all data sets.
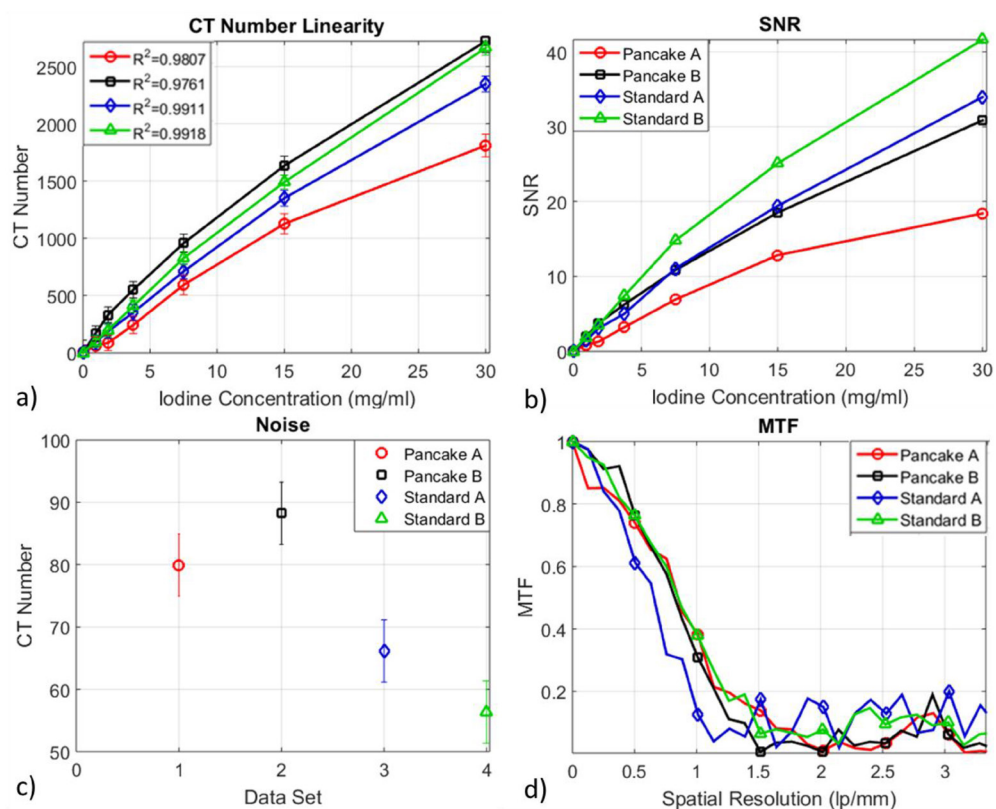
Figure 5. Comparison of the SARRP standard imaging geometry (standing phantom) versus 'pancake' imaging geometry (lying phantom) for Institution A and Institution B: (a) CT number linearity, (b) SNR, (c) noise, and (d) slanted edge MTF.

Table 5. Validation between SAPA and independent calculations.

	CT linearity R^2	Noise	SNR	MTF	Geometric accuracy Bead distance, voxel size	Contrast 30 mgI ml^{-1}
Difference	±0.0003	±5 HU	±3	±0.05	±0.20 mm, <1.0%	±10 HU

3.5. SAPA validation

QA test results determined by SAPA and independent calculations were compared and the differences are summarized in table 5. The maximum difference between the CT number linearity (R^2) as calculated by SAPA and Fiji was less than 0.0003. The noise and uniformity variations between the two methods were less than 5 HU. Geometric accuracy was calculated to be within ±0.20 mm of bead distance (the voxel size). The differences between SAPA and manual MTF and contrast were 0.05 and 2.3%, respectively, and thus all in good agreement. The average SAPA computation time for complete QA analysis for a 0.20 mm voxel, 400-slice microCT data set was less than 20 s using an Intel Core i7-6700HQ CPU 2.60 GHz quad-core laptop.

4. Discussion

MicroCT imaging of image-guided small animal irradiators has been investigated by analyzing the output of CT number linearity, SNR, noise and uniformity, geometric accuracy, spatial resolution, and contrast using the Shelley microCT phantom in a multi-institutional study.

Examples of the varying image quality for data acquired at different institutions and with different protocols are presented in figure 6. Displayed are the qualitative image difference of a scan from the uniformity plate that passed all tolerance levels (figure 6(a), Institution 4), and a scan that did not (figure 6(b), Institution 6), as a means for visual representation of acceptable image quality. Also presented are differences in the PXi X-RAD SmART image quality for images acquired in 60 s and 600 mAs (figure 6(c)) and 120 s and 360 mAs (figure 6(d)) with the same frame rate of 5 fps. Streaking artifacts were noticeable in all images acquired with imaging times of less than 120 s, regardless of the current-exposure time. With the standard acquisition frame rate of 5 fps and a full 360° projection for the PXI X-RAD SmART, this would correspond to a minimum of 600 frames per scan to avoid streaking artifacts.

CT number linearity directly affects the accuracy of dose calculations, which are based on microCT images of small animals. SNR, spatial resolution, noise, and uniformity are parameters that impact the ease of proper identification of small animal anatomical structures and also affect the accuracy of dose calculations. Geometric accuracy and contrast are crucial for accurate spatial targeting and measurements of anatomical structures, which can be used to determine how a tumor is responding to treatment.

The minimum SNR and noise passing tolerance levels were obtained with current-exposure times of 120 and 240 mAs for the PXi X-RAD SmART and Xstrahl SARRP systems, respectively. One may shorten the scanning time and increase the tube current (while maintaining the minimum recommended current-exposure time) to minimize motion artifacts caused by physiological motion of the animal. It should be considered that for the PXi X-RAD SmART system, images acquired in less than 120 s produced streaking artifacts. On the Xstrahl SARRP system, imaging time of less than 240 s resulted in high noise (>70 HU). The only data set that did not pass geometric accuracy had a total scanning time of less than 30 s, possibly failing due to image blurring caused by the relatively fast scan.

A user could theoretically increase the current-exposure time indefinitely to increase SNR and lower noise, but imaging time and dose must be taken into account, specifically in regards to scanning a live animal. High imaging doses may change the animal immune response and other biological pathways that may alter the experimental outcome (Boone *et al* 2004), so the lowest possible tube current (without compromising image quality) should be used with our recommended tube voltages. Thus, quantification of imaging dose should be an important part of system commissioning. Our recommended imaging parameters presented in table 4 result in an approximately 4 cGy imaging dose to an average size mouse with the Xstrahl SARRP system based on the user's manual, which states an imaging dose range between 1.2 cGy and 4.8 cGy. The manual of the PXi X-RAD SmART quotes a 'typical' imaging dose to be between 1 to 10 cGy to the center of a 30 mm thick small animal. MicroCT imaging dose to the various organs of small animals with varying imaging parameters in these commercial systems is not well established, and is currently being extensively examined in another study within our research group.

Due to the saturation of the Xstrahl SARRP detector, we were unable to obtain data with increased x-ray tube and current combinations higher than 80 kVp and 1 mA, and 60 kVp and 1.4 mA. The saturation of the Xstrahl SARRP detector is likely caused by the relatively short 50 cm SDD compared to the 64.5 cm SDD of the PXi X-RAD SmART system. In order
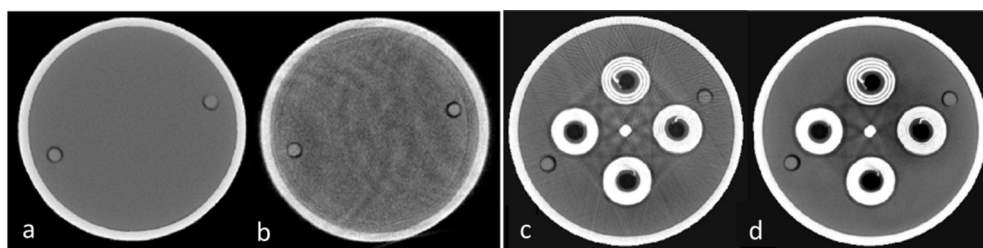
Figure 6. Uniformity plate scans displaying the image quality of (a) a scan that passed all recommended tolerance levels (Institution 4), and (b) a scan that did not (Institution 6). Streaking artifacts were present in an image (c) acquired with 60 s imaging time but not in an image (d) acquired with 120 s imaging time.

to keep image noise lower than the recommended value of 55 HU, a minimum current-exposure time of 240 mAs is recommended for the Xstrahl SARRP, and 180 mAs for the PXi X-RAD SmART. In an additional experiment, when the frame rate of the Xstrahl SARRP was increased from 6 to 12 fps, noise was lowered by 20%. It is also worth noting that Xstrahl SARRP images with voxel sizes of 0.275 mm and larger failed the spatial resolution test $(MTF(0.2) < 1.5 \text{ lp mm}^{-1})$. With the recommended voxel size of 200 μm, the highest achievable spatial resolution would be 2.5 lp mm^{-1}. We have experimentally verified, that at 20% MTF, the practically achievable spatial resolution was approximately 1.75 lp mm^{-1} for most systems. Assuming the small sizes of mouse anatomical structures in the order of 300–400 μm (for skull and vertebrae thickness, e.g.), we have decided to set the passing spatial resolution to 1.5 lp mm^{-1}, corresponding to resolving structures of 333 μm in size. It is important to have a high resolving power for bony structures not only for targeting and structure avoiding purposes, but also for dose calculations.

This work presents recommendations for imaging QA protocols for the two commercial systems for the benefit of approximately one hundred institutions owning them. We did not develop recommendations for QA imaging parameters for the two in-house small animal systems, because of their limited number of users and lack of multi-institutional data.

For the Xstrahl SARRP system, the standard imaging geometry (figure 3(c)) instead of the more natural 'pancake' geometry (figure 3(b), phantom laying on the SARRP couch) is recommend for imaging QA with the Shelley phantom using the Xstrahl SARRP system. In the 'pancake' geometry, the phantom rotates with respect to a stationary source, causing photons to traverse the longest part of the phantom. This increased attenuation and scatter, causing photon starvation artifacts that resulted in poorer image quality: scanning in the 'pancake' geometry consistently produced poorer CT number linearity (i.e. $R_p^2 = 0.976$, $R_s^2 = 0.992$), and up to 40% lower SNR and 35% higher noise, when compared to the standard imaging geometry. While small animals are often imaged and irradiated in the 'pancake' geometry, CT number linearity, SNR, and noise are poorer and less reproducible compared to the standard geometry. For this reason, we recommend scanning the Shelley phantom using standard geometry for the purpose of accurately quantifying image quality over time. Additionally, failing spatial resolution and noise were due to large voxel sizes (>0.275 mm), and insufficient tube current and scanning times, respectively. It should be noted that scanning small animals in the 'pancake' geometry would likely produce satisfactory image quality due to their smaller size compared to the Shelley phantom.

Quality control programs are a crucial part of the clinical radiotherapy process, and the same is true of the preclinical radiation therapy process. An important piece of a quality

control program is having tolerances for the tests that are performed. Despite the fact that these commercial small animal systems have been available for many years, there are no other (to our knowledge) studies which establish these specifications based on what can/is actually being achieved by these systems.

Users of the commercially available PXi X-RAD SmART and Xstrahl SARRP systems are encouraged to use QA imaging protocols summarized in table 4 for routine imaging QA with the Shelley phantom. With the recommended scanning protocols, the imaging tolerance levels presented in table 2 should be met for each test. Most importantly, a corrective action such as imaging system recalibration should be taken if tolerance levels cannot be met when the recommended imaging protocols are used.

5. Conclusions

We have developed the SAPA, automated image analysis software, tailored to microCT image quality analysis of the Shelley Micro-CT MCTP 610 phantom. Thanks to the multi-institutional data acquisition facilitated by the AAPM Working Group on Small Animal Irradiator Devices, we have analyzed microCT image quality from eleven institutions with image-guided small animal irradiators, and recommended imaging protocols and tolerance levels for routine image QA tests. This analysis provides a number of metrics to determine what is practically achievable for pre-treatment image quality in the interest of small animal radiotherapy. These metrics set a benchmark for what current users consider as acceptable quality, as well as present objective benchmarks to be met by updates to current and future small animal systems.

SAPA can be conveniently used to rapidly perform imaging QA tests using the Shelley phantom on any image-guided small animal irradiator, as well as microCT scanners. Additionally, SAPA can accumulate results over time and display possible changes in imaging functionality from its original performance and/or from the recommended tolerance levels presented in this work. This allows for corrective action to be made should image quality degrade over time. Upon request, SAPA will be distributed to users of image-guided small animal irradiators.

Acknowledgments

Conflict of interest

PL is listed as an inventor of the PXi X-Rad225Cx system, which is licensed to Precision x-ray for commercial development. TK is an employee of Xstrahl, Inc. MB-C has obtained research support from Xstrahl, Inc. for work unrelated to this manuscript.

ORCID

Ashley E Rubinstein ⓘ https://orcid.org/0000-0003-0221-4603

References

Abràmofff M D, Magalhães P J and Ram S J 2004 Image processing with ImageJ part II *Biophotonics Int.* **11** 36–43

Barton K L *et al* 2013 PD-0332991, a CDK4/6 inhibitor, significantly prolongs survival in a genetically engineered mouse model of brainstem glioma *PLoS One* **8** e77639

Baumann B C *et al* 2012 An integrated method for reproducible and accurate image-guided stereotactic cranial irradiation of brain tumors using the small animal radiation research platform *Transl. Oncol.* **5** 230–7

Bazalova M and Graves E E 2011 The importance of tissue segmentation for dose calculations for kilovoltage radiation therapy *Med. Phys.* **38** 3039–49

Bazalova M and Graves E E 2014 Engineering smal animal conformal radiotherapy systems *Engineering in Translational Medicine* vol 2, ed W Cai (Berlin: Springer) pp 853–75

Bissonnette J *et al* 2012 Quality assurance for image-guided radiation therapy utilizing CT-based technologies: a report of the AAPM TG-179 *Med. Phys.* **39** 1946–63

Boone J M, Velazquez O and Cherry S R 2004 Small-animal x-ray dose from micro-CT *Mol. Imaging* **3** 149–58

Burrell K *et al* 2013 A novel high-resolution *in vivo* imaging technique to study the dynamic response of intracranial structures to tumor growth and therapeutics *J. Vis. Exp.* **76** e50363

Chattopadhyay N *et al* 2013 Molecularly targeted gold nanoparticles enhance the radiation response of breast cancer cells and tumor xenografts to x-radiation *Breast Cancer Res. Treatment* **137** 81–91

Clarkson R *et al* 2011 Characterization of image quality and image-guidance performance of a preclinical microirradiator *Med. Phys.* **38** 845–56

Droege R T and Morin R L 1982 A practical method to measure the MTF of CT scanners *Med. Phys.* **9** 758–60

Du L Y *et al* 2007 A quality assurance phantom for the performance evaluation of volumetric micro-CT systems *Phys. Med. Biol.* **52** 7087–108

Herter-sprie G S *et al* 2014 Image-guided radiotherapy platform using single nodule conditional lung cancer mouse models *Nat. Commun.* **5** 1–8

Jensen M D *et al* 2013 Implementation and commissioning of an integrated micro-CT/RT system with computerized independent jaw collimation *Med. Phys.* **40** 081706

Judy P F 1976 The line spread function and modulation transfer function of a computed tomographic scanner *Med. Phys.* **3** 233–6

Kunjachan S *et al* 2015 Nanoparticle mediated tumor vascular distruption: a novel strategy in radiation therapy *Nano Lett.* **15** 7488–96

Lee D A *et al* 2013 Functional interrogation of adult hypothalamic neurogenesis with focal radiological inhibition *J. Vis. Exp.* **81** e50716

Lo V C K *et al* 2012 Beyond radiation therapy: photodynamic therapy maintains structural integrity of irradiated healthy and metastatically involved vertebrae in a pre-clinical *in vivo* model *Breast Cancer Res. Treat.* **135** 391–401

Mahmood J *et al* 2014 Targeting the renin-angiotensin system combined with an antioxidant is highly effective in mitigating radiation-induced lung damage *Int. J. Radiat. Oncol. Biol. Phys.* **89** 722–8

Redmond K J *et al* 2011 A radiotherapy technique to limit dose to neural progenitor cell niches without compromising tumor coverage *J. Neurooncol.* **104** 579–87

Rodriguez M *et al* 2009 Commissioning of a novel microCT/RT system for small animal conformal radiotherapy *Phys. Med. Biol.* **54** 3727–40

Schindelin J *et al* 2012 Fiji: an open-source platform for biological-image analysis *Nat. Methods* **9** 676–82

Tryggestad E *et al* 2009 A comprehensive system for dosimetric commissioning and Monte Carlo validation for the small animal radiation research platform *Phys. Med. Biol.* **54** 341–57

Van Hoof S J, Granton P V and Verhaegen F 2013 Development and validation of a treatment planning system for small animal radiotherapy: SmART-plan *Radiother. Oncol.* **109** 361–6

Verhaegen F, Granton P and Tryggestad E 2011 Small animal radiotherapy research platforms *Phys. Med. Biol.* **56** R55–83

Wong J *et al* 2008 High-resolution, small animal radiation research platform with x-ray tomographic guidance capabilities *Int. J. Radiat. Oncol. Biol. Phys.* **71** 1591–9

Zeng J *et al* 2013 Anti-PD-1 blockade and stereotactic radiation produce long-term survival in mice with intracranial gliomas *Int. J. Radiat. Oncol. Biol. Phys.* **86** 343–9

Zhou H *et al* 2010 Development of a micro-computed tomography-based image-guided conformal radiotherapy system for small animals *Int. J. Radiat. Oncol. Biol. Phys.* **78** 297–305